

Can we realize Kitaev quantum spin liquids in the $j_{\text{eff}} = 1/2$ honeycomb cobaltates?

Shreya Das,^{1,*} Sreekar Voleti,^{2,*} Tanusri Saha-Dasgupta,^{1,†} and Arun Paramekanti^{2,‡}

¹*Department of Condensed Matter Physics and Materials Science,
S.N. Bose National Centre for Basic Sciences, Kolkata 700098, India.*

²*Department of Physics, University of Toronto, Toronto, Ontario, M5S 1A7, Canada*

The quest for Kitaev quantum spin liquids has led to great interest in honeycomb quantum magnets with strong spin-orbit coupling. It has been recently proposed that even Mott insulators with $3d$ transition metal ions, having nominally weak spin-orbit coupling, can realize such exotic physics. Motivated by this, we study the rhombohedral honeycomb cobaltates CoTiO_3 , $\text{BaCo}_2(\text{PO}_4)_2$, and $\text{BaCo}_2(\text{AsO}_4)_2$, using *ab initio* density functional theory, which takes into account realistic crystal field distortions and chemical information, in conjunction with exact diagonalization numerics. We show that these Co^{2+} magnets host $j_{\text{eff}} = 1/2$ local moments with highly anisotropic g -factors, and we extract their full spin Hamiltonians including longer-range and anisotropic exchange couplings. For CoTiO_3 , we find a nearest-neighbor easy-plane ferromagnetic XXZ model with additional bond-dependent anisotropies and interlayer exchange, which supports three-dimensional (3D) Dirac nodal line magnons. In contrast, for $\text{BaCo}_2(\text{PO}_4)_2$ and $\text{BaCo}_2(\text{AsO}_4)_2$, we find a strongly suppressed interlayer coupling, and significant frustration from additional third-neighbor antiferromagnetic exchange mediated by P/As. Such bond-anisotropic J_1 - J_3 spin models can support collinear zig-zag or coplanar spiral ground states; we discuss their dynamical spin correlations which reveal a gapped Goldstone mode, and argue that the effective parameters of these pseudospin-1/2 models may be strongly renormalized by coupling to a low energy spin-exciton. Our results call for re-examining proposals for realizing Kitaev spin liquids in the honeycomb cobaltates.

I. INTRODUCTION

A significant effort has been invested in exploring material realizations of Kitaev's honeycomb quantum spin liquid model and its anyon excitations [1–4]. The initial work in this direction focussed mainly on the iridate honeycomb magnets which have strong spin-orbit coupling (SOC) [5–11]. At this point, the most promising candidate appears to be α - RuCl_3 [12–22], where intermediate in-plane Zeeman fields appear to lead to a plateau in the thermal Hall conductivity κ_{xy} [23], and quantum oscillations in the diagonal thermal conductivity κ_{xx} [24], which have been proposed as signatures of emergent Majorana fermion excitations in an insulating quantum magnet. Realizing such exotic physics in a wider range of quantum materials is clearly highly desirable.

This quest has led to great interest in honeycomb cobaltates, where the Co^{2+} ion in an octahedral crystal field environment has total spin $S = 3/2$ moment and an effective total orbital angular momentum $L = 1$, which are locked by spin-orbit coupling, leading to a $j_{\text{eff}} = 1/2$ pseudospin doublet ground state [25, 26]. These materials were proposed to host to dominant Kitaev exchange between neighboring pseudospins, rendering them candidates for quantum spin liquids. While this is an exciting proposal, SOC is much weaker for $3d$ transition metal ions as compared with the $5d$ -iridates or $4d$ -ruthenates. As a result, trigonal distortions of the local crystal field environment, inevitable in any layered honeycomb mate-

rial, may be expected to have a considerable impact on the nature of exchange interactions and the low energy fate of magnetism in these materials.

To critically examine this issue, we explore several rhombohedral d^7 cobaltates — CoTiO_3 , $\text{BaCo}_2(\text{PO}_4)_2$, and $\text{BaCo}_2(\text{AsO}_4)_2$ — which are formed from stacked honeycomb Co^{2+} layers as shown in Fig. 1. In particular, we ask: does a realistic theory of the d^7 cobaltates, using a combination of *ab initio* density functional theory (DFT) and exact diagonalization numerics, favor the realization of Kitaev spin liquids in these materials?

A quick summary of our key results are as follows. Our *ab initio* computations reveal that although all three compounds host the stacked honeycomb Co^{2+} layers, the difference in the geometry and chemical composition of the spacer layers between the Co^{2+} layers greatly influences the resulting electronic structure of the three compounds. In CoTiO_3 , strong Co-Ti covalency leads to a more 3D electronic structure, while the delicate Co-As/P covalency and large separation between the Co^{2+} layers leads to weakly coupled 2D layers but with longer-range hoppings in the electronic structure of $\text{BaCo}_2(\text{AsO}_4)_2$ and $\text{BaCo}_2(\text{PO}_4)_2$. We use these DFT inputs to carry out an exact diagonalization study incorporating correlation effects, which has been shown to work well in other Mott insulators with SOC [21, 27]. Our exact diagonalization numerics reveal that the Co^{2+} ion has strongly anisotropic g -factors, consistent with experimental data [28–30]. For CoTiO_3 , our computations reveal a dominant nearest-neighbor XXZ easy-plane ferromagnetic coupling, with additional anisotropic compass-type exchange interactions and interlayer couplings. Such a spin Hamiltonian supports 3D Dirac nodal line magnon excitations and is in good quanti-

* These authors contributed equally

† tanusri@bose.res.in

‡ arunp@physics.utoronto.ca

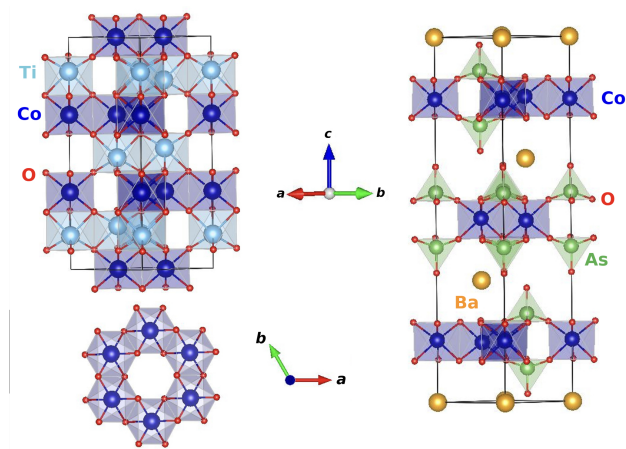


FIG. 1. Crystal structure of CoTiO_3 (left) and $\text{BaCo}_2(\text{AsO}_4)_2$ (right) viewed with hexagonal c -axis pointing upwards. The Co, Ti, As, Ba and O atoms are labeled and colored differently. Marked is the six formula unit hexagonal unit cell. Bottom left panel shows the top view of CoTiO_3 looking down the c -axis.

tative agreement with recent neutron scattering experiments [29, 30]. For $\text{BaCo}_2(\text{PO}_4)_2$ and $\text{BaCo}_2(\text{AsO}_4)_2$, we find that the spacer layers lead to nearly decoupled honeycomb layers. The magnetic Hamiltonian is found to be a quasi-2D easy-plane XXZ model with significant frustration from third-neighbor antiferromagnetic exchange. Such J_1 - J_3 honeycomb lattice spin models can support collinear zig-zag or coplanar spiral ground states [31]. We present results on their dynamical spin structure factor which reveals a gapped Goldstone mode arising from bond-dependent compass anisotropy terms. This is in qualitative agreement with neutron scattering results [32, 33]. Our results highlight the significant sensitivity of the magnetic Hamiltonian of the honeycomb cobaltates to the local crystal field environment and spacer layers which can mediate longer-range interactions, suggesting that fine-tuning of the chemistry and crystal fields may be needed to realize Kitaev spin liquids in these materials.

II. CRYSTAL STRUCTURE

All three compounds CoTiO_3 , $\text{BaCo}_2(\text{AsO}_4)_2$, and $\text{BaCo}_2(\text{PO}_4)_2$ crystallize in the rhombohedral $R\bar{3}$ space group. While the basic structural motif of all three compounds consist of stacked honeycomb cobaltate layers formed by edge shared CoO_6 octahedra, the out of plane stacking involving spacer layers between honeycomb planes are distinctly different between CoTiO_3 , and $\text{BaCo}_2(\text{AsO}_4)_2$ or $\text{BaCo}_2(\text{PO}_4)_2$. The left and middle panels of Fig. 1 show the crystal structures of CoTiO_3 and $\text{BaCo}_2(\text{AsO}_4)_2$, respectively; the crystal structure of $\text{BaCo}_2(\text{PO}_4)_2$ being very similar to that of $\text{BaCo}_2(\text{AsO}_4)_2$, is not shown. In case of CoTiO_3 , the

cobalt layers are separated by Ti layers, where octahedrally coordinated Ti^{4+} ions face share with CoO_6 octahedra along the hexagonal c -axis, with the Ti ion on top of Co ion, vertically displaced by 2.67\AA . In case of $\text{BaCo}_2(\text{AsO}_4)_2$, on the other hand, the Co layers are separated by bilayers of AsO_4 tetrahedra, one pointing up and another pointing down, and separated by large Ba^{2+} ions. This difference in spacer layer thickness between CoTiO_3 and the Ba compounds, makes the c -axis lattice constant of $\text{BaCo}_2(\text{AsO}_4)_2$ and $\text{BaCo}_2(\text{PO}_4)_2$ significantly different from CoTiO_3 , being 13.92\AA for CoTiO_3 , 23.49\AA for $\text{BaCo}_2(\text{AsO}_4)_2$, and 23.22\AA for $\text{BaCo}_2(\text{PO}_4)_2$. However, their inplane lattice constants are rather similar: 5.06\AA for CoTiO_3 , 5.00\AA for $\text{BaCo}_2(\text{AsO}_4)_2$, and 4.86\AA for $\text{BaCo}_2(\text{PO}_4)_2$. This gives rise to a more 2D character of the Co network in Ba compounds, while CoTiO_3 has more 3D character. Furthermore, as opposed to face-shared geometry of Co-Ti network, the AsO_4 tetrahedra corner share with CoO_6 octahedra, the As ion being displaced from Co ion by 1.67\AA along the in-plane directions and 1.41\AA along the vertical direction. This creates O-As-O bridges both from top and bottom between long ranged in-plane Co neighbors, this feature being absent for CoTiO_3 compound. These structural details have important implications for the electronic structure and low-energy Hamiltonian of the three compounds which we discuss next.

III. ELECTRONIC STRUCTURE

To characterize the valences, spin states, and orbital contributions of various ions, we first carry out the spin-polarized DFT calculations within the framework of generalized gradient approximation (GGA) [34]. See Supplementary Materials (SM) [35] for calculation details [36–38]. The magnetic moment of Co site is found to be around $2.60\mu_B$ confirming the high spin d^7 configuration of Co ions. Interestingly for CoTiO_3 , large fraction of the missing moment is found to be at Ti and O sites of $0.12\mu_B$ and $0.10\mu_B$, respectively, despite the nominally nonmagnetic configuration of Ti^{4+} and O^{2-} , indicating strong Co-O, and Ti-O covalency. For the Ba compounds, a similar magnitude of missing moment ($\sim 0.10\mu_B$) is found at O sites. Furthermore, a non-negligible moment of $\sim 0.05\mu_B$ is also found at the nominally valenced $\text{As}^{5+}/\text{P}^{5+}$ sites, indicating the subtle role of As/P in describing the electronic structure of the Ba compounds. Repeating the calculations within the GGA+SOC approach uncovers a substantial orbital moment of 0.16 - $0.17\mu_B$ at the Co site highlighting importance of SOC in these compounds. In order to check the effect of missing correlation effect beyond GGA, GGA with supplemented Hubbard U correction [39] within the framework of GGA+ U and GGA+SOC+ U was carried out with choice of $U=3$ eV and $J_H=0.7$ eV [40, 41], and we found that the results were qualitatively unchanged.

Since our goal is to use the DFT calculations to de-

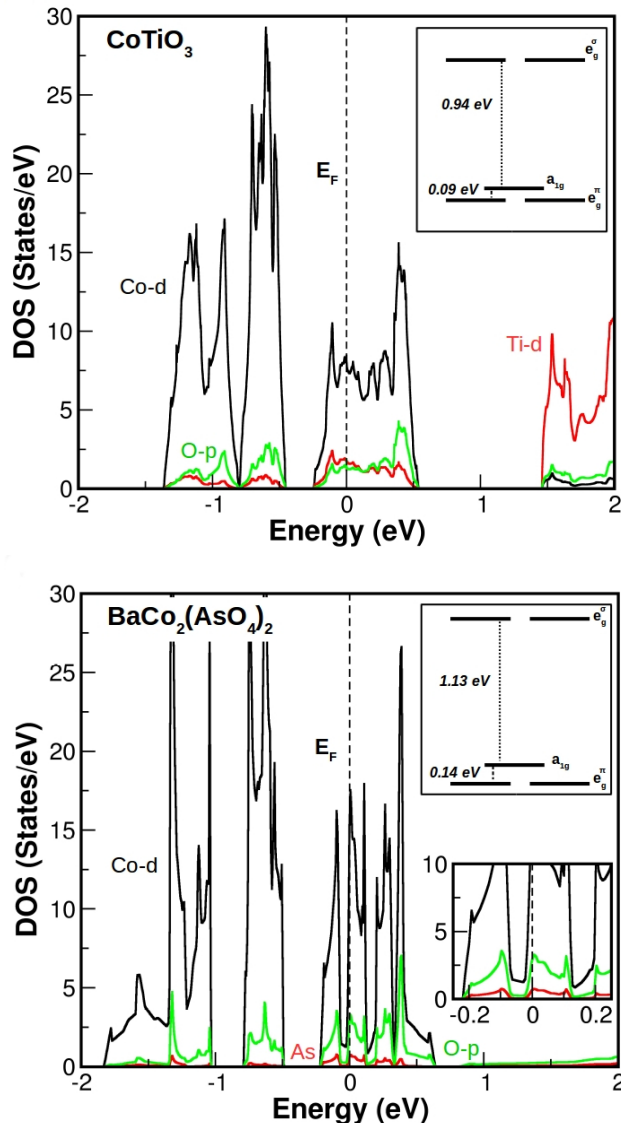


FIG. 2. Non spin-polarized DFT density of states of CoTiO_3 (top) and $\text{BaCo}_2(\text{AsO}_4)_2$ (bottom) projected to Co-d , Ti-d , As and O-p states. The zero of the energy is marked at the corresponding Fermi level (E_F). Crystal field splitting of the Co-d states are shown as insets. The second inset in bottom is the zoomed-in plot of the density of states close to E_F .

rive a low-energy Hamiltonian to be used as an input for a model Hamiltonian study, we henceforth focus on the non-spin-polarized electronic structure of these compounds. Fig. 2 shows the density of states of CoTiO_3 and $\text{BaCo}_2(\text{AsO}_4)_2$ compounds projected to different orbital characters; the electronic structure of $\text{BaCo}_2(\text{PO}_4)_2$ is very similar to $\text{BaCo}_2(\text{AsO}_4)_2$ and is thus not shown. In an ideal octahedral environment the $\text{Co } d$ states are split into three-fold degenerate t_{2g} and two-fold degenerate e_g states. However, the CoO_6 octahedra in the studied compounds are not perfect, rather they are trigonally distorted with the Co atom moved along $[111]$ direction from

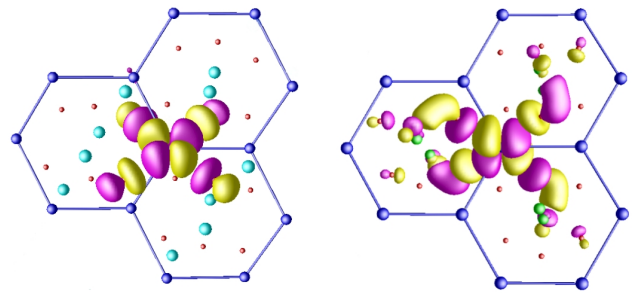


FIG. 3. In-plane view of NMTO downfolded $\text{Co } d_{x^2-y^2}$ Wannier function of CoTiO_3 (left) and $\text{BaCo}_2(\text{AsO}_4)_2$ (right). Plotted are the constant value isosurfaces with lobes of opposite signs colored as magenta and yellow. The hexagonal network of Co atoms in blue is shown, with O and Ti/As atoms shown as small-red and medium-cyan/green balls.

the centre of the octahedra, leading to three short and three long Co-O bonds. As shown in the insets of Fig. 2, this further splits the d levels into two-fold degenerate e_g^π , non-degenerate a_{1g} , and two-fold degenerate e_g^σ levels. The octahedral splitting is found to be about ~ 1 eV, while trigonal splitting is found to be ~ 0.1 eV and thus larger than the nominal SOC on Co . Within the non-spin-polarized scheme of calculations, the $\text{Co } t_{2g}$ are fully occupied while the $\text{Co } e_g$ states are partially filled. As seen from the density of states near the Fermi level, there is significantly contribution of $\text{O } p$ states along with the $\text{Co } d$ states, indicating strong Co-O covalency; this was also manifest in the presence of substantial magnetic moment at the otherwise non-magnetic O sites. In CoTiO_3 , we also notice a significant presence of Ti-d character near the Fermi level, which we deem responsible for the 3D nature of the density of states. While the density of states of $\text{BaCo}_2(\text{AsO}_4)_2$ bears an overall resemblance to that of CoTiO_3 , the details are markedly different. Near the Fermi level, we find the appearance of pseudogap like features seen in the inset of the bottom panel of Fig. 2, which arises due to intricate interplay of long-ranged in plane Co-Co interactions mediated by As ; this feature is absent in CoTiO_3 . While the contribution of As states near the Fermi level is small compared to Ti , it is still non-negligible as highlighted in the zoomed-in plot of the density of states in the second inset of the bottom panel of Fig. 2. As discussed below, we believe this overlap with As states drives the overlap of further neighbor Wannier orbitals in the Ba compounds and leads to strong third-neighbor exchange.

IV. LOW-ENERGY DFT HAMILTONIAN

In an attempt to derive $\text{Co } d$ -only low energy Hamiltonian out of DFT calculations, we resort to the energy selective N -th order muffin-tin orbital (NMTO) based downfolding technique [42]. Starting from a self-consistent DFT calculation in linear muffin-tin orbital

basis,[43], NMTO-downfolding calculation arrives at a low-energy Co d -only Hamiltonian by integrating out degrees that are not of interest like O- p , Ti- d , As and Ba states. This procedure constructs the ab-initio derived effective Co Wannier functions, the head parts of which are shaped according to Co d symmetries, while the tail parts are shaped according to the integrated out degrees of freedom which are mixed in with Co d characters. The construction of these effective Wannier functions depends on the choice of basis. We chose the octahedral local coordinate system with z -axis of the local coordinate system pointed along one of short Co-O bond, and the local y -axis pointed closet to neighboring Co-O bond. With this choice, the local z -axis on nearest neighbor edge-shared Co pairs point in opposite directions, with the center of inversion at the middle of the vector connecting the Co-Co pair. Fig. 3 shows a representative example of the effective Co $d_{x^2-y^2}$ Wannier function as given by NMTO-downfolded calculations for CoTiO₃ and BaCo₂(AsO₄)₂, which exhibits $pd\sigma$ antibonds formed between Co and O, which appear as pronounced tails shaped according to O p symmetry. In the case of CoTiO₃, a significant weight of the tail also sits at the out-of-plane Ti site, as we find from other Wannier orbitals (not shown). What is remarkable in case of Ba compound is that one of the lobes of the O-tail bends towards As sites due to overlap of Co-O and As-O covalency at the corner-shared O site of CoO₆ octahedra and AsO₄ tetrahedra. This As-covalency driven bending of the tails promotes the long-ranged third neighbor in-plane Co-Co interaction, which plays an important role in the spin model for BaCo₂(AsO₄)₂; we find similar features in BaCo₂(PO₄)₂.

The low-energy tight-binding Hamiltonian, in the basis of NMTO-downfolded effective Co d Wannier functions, encodes the effect of local distortion of CoO₆ octahedra, as well as the effect of spacer chemistry and geometry. The full local crystal field matrix and the hopping matrices for various neighbors are given in the SM [35]. This information is next used to build model Hamiltonians for these cobaltates.

V. EXACT DIAGONALIZATION RESULTS: SINGLE ION PROPERTIES

From our DFT calculations, we extract a local crystal field Hamiltonian H_{CF} describing the d -orbital manifold of the Co²⁺ ion in a distorted octahedral crystal field environment which only has a residual C_3 symmetry. We supplement this Hamiltonian with SOC and interactions, so that the on-site Hamiltonian takes the form

$$H_{\text{loc}} = \xi H_{\text{CF}} + H_{\text{SOC}} + H_{\text{int}}. \quad (1)$$

Here, H_{SOC} is the single-particle SOC term, explicitly given by

$$H_{\text{SOC}} = \lambda \sum_{\ell\ell'm} \sum_{\alpha\beta} c_{\ell s}^\dagger L_{\ell\ell'}^m c_{\ell' s'} \sigma_{ss'}^m, \quad (2)$$

where (ℓ, ℓ') are orbital labels corresponding to $\{(yz, xz, xy), (x^2-y^2, 3z^2-r^2)\}$, m labels the vector component of the orbital L or spin σ angular momentum, with s, s' being spin component labels. H_{int} is the spherically symmetric Kanamori Hamiltonian encoding interactions between the electrons:

$$H_{\text{int}} = U \sum_{\ell} n_{\ell\uparrow} n_{\ell\downarrow} + U' \sum_{\ell > \ell'} n_{\ell} n_{\ell'} - J_H \sum_{\ell \neq \ell'} \mathbf{S}_{\ell} \cdot \mathbf{S}_{\ell'} + J_H \sum_{\ell \neq \ell'} c_{\ell\uparrow}^\dagger c_{\ell\downarrow}^\dagger c_{\ell'\downarrow} c_{\ell'\uparrow}. \quad (3)$$

Here, U , U' , and J_H represent intra-orbital Hubbard, inter-orbital Hubbard, and Hund's couplings, respectively, and the spin operator in orbital ℓ is

$$\mathbf{S}_{\ell}^m = \frac{1}{2} c_{\ell s}^\dagger \sigma_{ss'}^m c_{\ell s'}. \quad (4)$$

We assume $U' = U - 2J_H$ as appropriate for a spherically symmetric Coulomb interaction [44]. Finally, in this single-ion Hamiltonian Eq. 1, we have incorporated a scaling factor ξ multiplying the H_{CF} obtained from our DFT calculations, as a crude way to account for the ‘‘double counting’’ of interactions. We refer here to the fact that *ab initio* calculations partially account for inter-orbital repulsion and changes in the corresponding orbital occupancies and energies at mean field level, while such a renormalization of crystal field levels will also occur from the full set of Kanamori interactions in Eq. 3.

Below, we set $\lambda = 80 \text{ meV}$ for Co²⁺ [45], and choose the scaling factor $\xi = 0.65$. Based on an exploration of how the different exchange couplings vary with interactions (discussed below), we fix the interaction strengths to $U = 3.25 \text{ eV}$ and $J_H = 0.7 \text{ eV}$ [46]. We find that this set of parameters leads to reasonable results for the single ion g -factors, as well as the low energy single ion excitations and spin-wave modes observed in CoTiO₃ using inelastic neutron scattering experiments [29, 30]. We have found that the exchange Hamiltonians we derive in later sections are not substantially impacted by the precise value of ξ .

A. Kramers doublet ground state

As discussed in Ref [25], the $3d^7$ Co²⁺ ion in an octahedral crystal field environment is predominantly in the high-spin $S = 3/2$ ($t_{2g}^5 e_g^2$) configuration. Combining this with the total effective orbital angular momentum $L = 1$, of a single hole in the t_{2g} orbitals, the SOC term with $\lambda > 0$ stabilizes a $j_{\text{eff}} = 1/2$ pseudospin degree of freedom. Indeed, our exact diagonalization of the Hamiltonian leads to a Kramers doublet ground state for a wide range of parameter values, indicating that such a pseudospin-1/2 picture remains valid for all three cobaltates even in the presence of realistic distortions.

Material	g_{\perp}	g_{\parallel}
CoTiO ₃	5.0	3.2
BaCo ₂ (AsO ₄) ₂	5.0	2.7
BaCo ₂ (PO ₄) ₂	5.0	3.0

TABLE I. Computed g -factors corresponding to directions perpendicular (in-plane) or parallel (out-of-plane) to the C_3 axis (c -axis) for honeycomb cobaltates studied in this paper.

B. Single-ion excitations

Inelastic neutron scattering experiments on CoTiO₃ reveal magnetic excitations above the $j_{\text{eff}} = 1/2$ doublet at energies $\{29(2), 58(7), \dots, 132(3)\}$ meV, where “...” indicates a broad continuum of significant scattering intensity in the 60-120 meV range where individual sharp peaks cannot be resolved [29, 30]. Choosing the scaling factor $\xi = 0.65$ in H_{loc} , we find that these low-lying many-body crystal field excitations above the $j_{\text{eff}} = 1/2$ doublet ground state in CoTiO₃ are at energies $\{\underline{22}, \underline{63}, 104, 111, \underline{132}\}$ meV, with the underlined excitations energy levels being in reasonably good agreement with the experimentally observed peaks. We contrast these results with the corresponding values when the scale factor is set to $\xi = 1$, which leads to excitation energies $\{15, 84, 118, 130, 152\}$ meV quite unlike the data.

Using this scaling factor $\xi = 0.65$ for BaCo₂(AsO₄)₂ and BaCo₂(PO₄)₂, we find the excited states at excitation energies which are respectively at $\{14, 85, 120, 134, 158\}$ and $\{16, 77, 112, 126, 151\}$. These could be explored in future experiments. We note that similar spin exciton states have also been measured in certain pyrochlore cobaltates [47].

C. g -factors

Table I lists the g -factors associated with this pseudospin degree of freedom which we obtain from the ground state expectation value $2\langle(\vec{L} + 2\vec{S})\rangle$ in the presence of a weak Zeeman field \vec{B} . By choosing \vec{B} to point perpendicular or parallel to the C_3 axis (i.e., c -axis), we extract g_{\perp} and g_{\parallel} respectively. In contrast to the isotropic g -factors obtained for the iridate d^5 Mott insulators, all the cobaltates studied here show highly anisotropic g -factors, in agreement with recent experiments [28, 33]. Such anisotropic g -factors have also been measured in certain pyrochlore cobaltates [47]. To the best of our knowledge, g -factors for BaCo₂(PO₄)₂ have not been measured; our estimates may be compared with future experiments.

VI. PERTURBATION THEORY FOR INTER-SITE EXCHANGE

In order to obtain the exchange interactions between pseudospins on a pair of sites, we use the single-ion energy levels and eigenfunctions and incorporate inter-site hopping to second order in perturbation theory. We outline this below, together with a brief discussion about the dependence on the various exchange couplings on interaction parameters such as U and J_H , with further details given in the SM [35].

A. Two-site perturbation theory

The interactions between the pseudospins can be obtained via second order perturbation theory, using hopping integrals extracted from the above DFT calculations. The calculation schematically proceeds as follows. (i) We solve the single site problem for occupancies d^6 , d^7 and d^8 , to obtain the full set of energy levels and many-body wavefunctions including SOC. In doing this, we apply a weak field along the global Z -axis (C_3 axis perpendicular to the honeycomb planes) in order to define our pseudospin $|\uparrow\rangle, |\downarrow\rangle$ basis states (see Fig. 4, reproduced from [5]). (ii) We extract spin-independent hopping matrices $T^{(ij)}$ from DFT, whose elements $T_{\ell\ell'}^{(ij)}$ describe an electron in orbital ℓ at site i hopping to an orbital ℓ' at site j , so that the (ij) kinetic energy is

$$\hat{T}_{ij} = \sum_{\ell\ell'\alpha} (T_{\ell\ell'}^{(ij)} c_{j\ell'\alpha}^\dagger c_{i\ell\alpha} + T_{\ell'\ell}^{(ji)} c_{i\ell\alpha}^\dagger c_{j\ell'\alpha}) \quad (5)$$

(iii) We focus on initial and final states where each of the two sites live in a ground doublet which we denote as $|b\rangle, |b'\rangle$. These kets span a 4-dimensional Hilbert space, formed by the direct product of doublet levels at each site. The operator \hat{T}_{ij} connects these states to intermediate many-body levels (d^6, d^8) or (d^8, d^6) which we denote as $|e\rangle$. (iv) From second order perturbation theory, we obtain the effective Hamiltonian as

$$\left[\mathcal{H}_{\text{eff}}^{(2)}\right]_{b',b} = \sum_e \frac{\langle b' | \hat{T}_{ij} | e \rangle \langle e | \hat{T}_{ij} | b \rangle}{E_b - E_e} \quad (6)$$

where E_e and $E_b = E_{b'}$ refer to the energies of the intermediate and initial/final ground states, respectively. $\mathcal{H}_{\text{eff}}^{(2)}$ is a 4x4 matrix, describing the interactions between the doublet manifolds on the two sites. (v) Finally, from this 4x4 Hamiltonian, the exchange matrix \mathcal{J} is extracted by writing $\mathcal{H}_{\text{eff}}^{(2)}$ above as a pseudospin exchange term

$$\mathcal{H}^{ij} = \sum_{\alpha\beta} \mathcal{S}_{\alpha}^i \mathcal{J}_{\alpha\beta}^{ij} \mathcal{S}_{\beta}^j \quad (7)$$

where α and β are the components of the spin vectors, and the \mathcal{S}_{α} are pseudospin-1/2 operators.

For instance, along a C -type nearest-neighbor bond (see left panel in Fig.4), the exchange matrix $\mathcal{J}[C]$ is

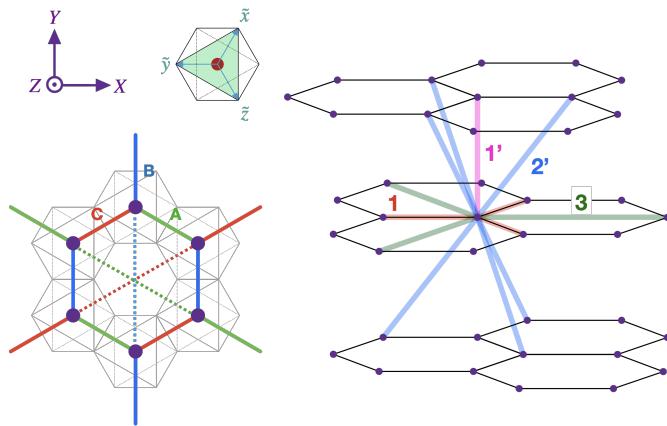


FIG. 4. (Left) The honeycomb plane is shown, as viewed down the c axis, along with the global XYZ and local $\tilde{x}\tilde{y}\tilde{z}$ basis. The definition of the bases, along with that of the A , B , and C bonds is consistent with Ref. [5]. The dotted bonds denote the third-nearest neighbor bonds, which can be also be defined as A , B , C -type. (Right) Bonds with non-negligible exchange couplings for the different materials; unprimed numbers refer to in-plane neighbors, while primed numbers refer to the out-of-plane neighbors.

defined as

$$\mathcal{J}[C] = \begin{pmatrix} J^{XY} + D & E & G \\ E & J^{XY} - D & F \\ G & F & J^Z \end{pmatrix} \quad (8)$$

with antisymmetric terms, e.g. Dzyaloshinskii-Moriya (DM) exchange couplings, being forbidden by inversion symmetry about the bond center. We can extract the corresponding exchange matrices $\mathcal{J}[A]$ and $\mathcal{J}[B]$ on the A -type and B -type bonds simply by a $\pm 2\pi/3$ rotations of the above exchange matrix about the C_3 axis. More generally, the exchange matrices on generic bonds would allow DM terms, but we find that these are negligible, even for bonds where there is no center of inversion (eg. second-neighbor bonds 2 and 2').

In Appendix A, we present results for the exchange matrices in terms of the ideal local octahedral basis in which the famous Kitaev- Γ type Hamiltonians are usually formulated (also shown in the left panel in Fig.4). However, we note that in all the cobaltates we have examined, the pseudospin Hamiltonian is simplest in the above global basis, i.e. with the fewest number of nonzero entries in the exchange matrices.

B. Dependence of Exchanges on Interaction Parameters

The spin exchange interactions are sensitive to the interaction parameters U, J_H in Equation (3). To illustrate this, Fig. 5 shows the dependence of the first-neighbor XY exchange J_1^{XY} on the Hubbard U repulsion for all three cobaltates, while the inset displays the variation of

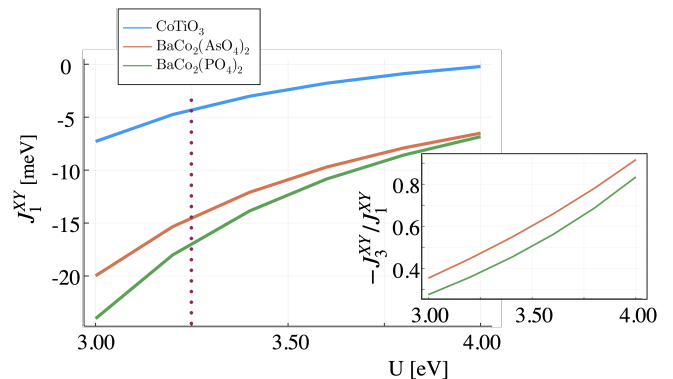


FIG. 5. Dependence of the nearest-neighbor exchange interaction J_1^{XY} on the Hubbard U , for fixed $J_H = 0.7$ eV. For $U = 3.25$ eV (shown by the dotted line), the exchange couplings for CoTiO_3 are in good agreement with neutron experiments [29, 30]. Inset shows the ratio $-J_3^{XY}/J_1^{XY}$ over the same range of U for the Barium compounds, suggesting significant frustration from third neighbor exchange. The full set of significant exchange couplings for $U = 3.25$ and $J_H = 0.7$ eV are quoted in Tables II, III, and IV.

the non-negligible third-neighbor exchange $-J_3^{XY}/J_1^{XY}$ in $\text{BaCo}_2(\text{AsO}_4)_2$ and $\text{BaCo}_2(\text{PO}_4)_2$. The SM [35] includes additional plots for the J_H dependence of these exchange couplings, as well as the (U, J_H) dependence of bond-dependent anisotropies and further neighbor interactions.

Based on Fig. 5, and similar plots, we find that a reasonable choice of $U = 3.25$ eV and $J_H = 0.7$ eV [40, 41] leads to exchange couplings for CoTiO_3 which are in excellent agreement with inelastic neutron scattering experiments. For $\text{BaCo}_2(\text{AsO}_4)_2$ and $\text{BaCo}_2(\text{PO}_4)_2$, however, the spin ground state is extremely sensitive to the third-neighbor exchange over a range of J_3^{XY}/J_1^{XY} (shown in the inset of Fig. 5). This suggests that some degree of fine-tuning might be needed to explain their precise magnetic ordering. Indeed, experiments on $\text{BaCo}_2(\text{PO}_4)_2$ have even argued for the coexistence of orderings with different wavevectors in the same sample. In addition to this issue, we find a much larger overall scale of the exchange couplings in these two materials when compared with experimental reports - we later discuss a possible reason for this significant discrepancy.

VII. SPIN HAMILTONIANS, ORDERED STATES, SPIN DYNAMICS

A. CoTiO_3

We find that the spin model in CoTiO_3 is best described as a nearest-neighbor ferromagnetic easy-plane XXZ model with significant compass-type anisotropies in the honeycomb plane, along with a weaker antiferromagnetic coupling between honeycomb layers. The full set of significant exchange coupling values are listed in

Table II. This complete set of spin interactions favors an ordered ground state where the moments have XY ferromagnetic order within each honeycomb layer, but are antiferromagnetically stacked from one layer to the next. The interlayer exchanges are mediated by the significant overlap of the Co Wannier orbitals with the spacer Ti ions. The first-neighbor exchange coupling and its strong anisotropy, as well as the weaker interlayer couplings, are in very good agreement with those inferred from neutron scattering studies of the material [29, 30]. The scale of the compass anisotropy terms are also consistent with those conjectured in previous studies.

Fig. 6 shows the linear spin wave dispersion, obtained with our computed exchange interactions, along specific cuts in momentum space. The left panel reveals a Goldstone mode at the zone center - this is an artefact of linear spin wave theory, since the significant anisotropic “compass”-type exchange couplings D and E break the $U(1)$ symmetry of the pure XXZ model. Order by disorder physics, beyond linear spin-wave theory, is expected to pin the ordered moment and gap out the Goldstone mode [30]. The right panel shows the computed Dirac node which has been observed in inelastic neutron scattering experiments; we find that this node is shifted away from the Brillouin zone corner which is at $(2/3, 2/3, 1/2)$ (dotted line in the right panel of Figure 6). This is in accordance with predictions that there are 3D Dirac nodal lines which should wind, like a triple helix, around the $(2/3, 2/3, L)$ axis in momentum space. This displacement of the Dirac nodal lines is enabled by the anisotropic D and E exchange couplings, and might lead to a suppression of the magnon density of states, as seen in recent experiments [30].

B. $\text{BaCo}_2(\text{AsO}_4)_2$ and $\text{BaCo}_2(\text{PO}_4)_2$

The Barium compounds are much more two-dimensional compared to CoTiO_3 , with extremely small inter-layer couplings $\lesssim 0.1$ meV. The source of this layer decoupling is the large inter-plane distances discussed in Section II. In addition, the less buckled nature of the honeycomb planes and the Wannier orbital overlap with As/P appears to promote larger in-plane hopping amplitudes. As a result, we find that the computed exchange interactions between $j=1/2$ pseudospins in these compounds are significantly enhanced compared with

CoTiO_3	Bond-1	Bond-1'	Bond-2'
J^{XY}	-4.5 meV	0.4 meV	0.8 meV
J^Z	-0.3 meV	0.3 meV	0.4 meV
D	1.8 meV	~ 0	~ 0
E	-2.2 meV	~ 0	~ 0

TABLE II. Table of dominant exchange parameters for CoTiO_3 , corresponding to $U = 3.25$ eV and $J_H = 0.7$ eV. For the definitions of the bonds, see Fig. 4 (right panel).

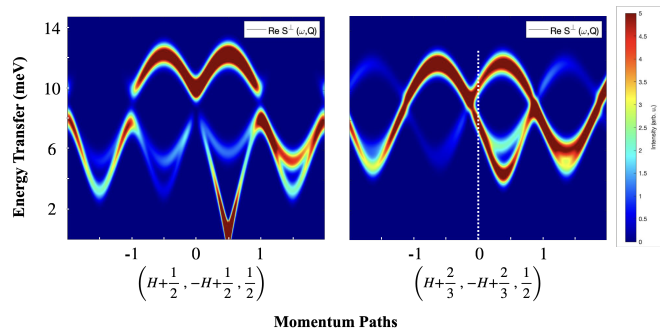


FIG. 6. Spin wave dispersions for CoTiO_3 , obtained using SpinW [48], plotted along two cuts in momentum space in the $L = 1/2$ plane [29, 30]. Dotted line in right panel denotes the Brillouin zone corner.

CoTiO_3 .

Tables III and IV show values for the exchange parameters for the $\text{BaCo}_2(\text{AsO}_4)_2$ and $\text{BaCo}_2(\text{PO}_4)_2$ respectively. The first-neighbor interaction leads to an easy-plane XXZ model, but with subdominant anisotropies, which is qualitatively similar to CoTiO_3 . However, in contrast to CoTiO_3 we find strong frustration coming from significant third-neighbor antiferromagnetic exchange; this leads to antiferromagnetic XY ground states in the Barium compounds.

The well-known classical phase diagram of the $J_1 - J_3$ model (see Appendix B for a phase diagram reproduced from [31]) features a tiny sliver ($-J_3/J_1 \sim 0.25 - 0.4$) of an incommensurate coplanar spiral phase sandwiched between the more robust ferromagnetic and zig-zag ordered phases. Based on our exploration of how the exchange couplings vary with the interaction parameters in Eq. 3 (see Figure 5), we find that the ratio J_3/J_1 lies close to this window. We thus deduce that the ground states of these materials could be extremely sensitive to small variations in material parameters.

Based on our computed exchange couplings shown in Tables III and IV, we extract the Curie-Weiss constants for $\text{BaCo}_2(\text{AsO}_4)_2$ and $\text{BaCo}_2(\text{PO}_4)_2$ both parallel to the c -axis, and perpendicular to the c -axis (i.e., in the honeycomb plane). For $\text{BaCo}_2(\text{AsO}_4)_2$, we find $\Theta_{\parallel} \simeq 65$ K and $\Theta_{\perp} \simeq 4$ K, about twice as large as the corresponding experimental values [28]. For $\text{BaCo}_2(\text{PO}_4)_2$, we find $\Theta_{\parallel} \simeq 90$ K and $\Theta_{\perp} \simeq 23$ K, which remains to be experimentally studied on single crystal samples.

$\text{BaCo}_2(\text{AsO}_4)_2$	Bond-1	Bond-3
J^{XY}	-14.5 meV	7.1 meV
J^Z	-3.8 meV	2.3 meV
D	1.5 meV	~ 0
E	-1.7 meV	~ 0

TABLE III. Table of dominant exchange parameters for $\text{BaCo}_2(\text{AsO}_4)_2$, corresponding to $U = 3.25$ eV and $J_H = 0.7$ eV. For the definitions of the bonds, see Fig. 4 (right panel).

$\text{BaCo}_2(\text{PO}_4)_2$	Bond-1	Bond-3
J^{XY}	-17.3 meV	6.9 meV
J^Z	-5.0 meV	2.4 meV
D	-2.7 meV	~ 0
E	0.2 meV	~ 0

TABLE IV. Table of dominant exchange parameters for $\text{BaCo}_2(\text{PO}_4)_2$, corresponding to $U = 3.25$ eV and $J_H = 0.7$ eV. For the definitions of the bonds, see Fig. 4 (right panel).

Using SpinW [48], we have computed the magnetic order and dynamical spin correlations corresponding to the exchange values in Tables III. We find that this parameter set supports zig-zag magnetic order as shown in Fig. 7 (left panel), with moment directions as shown for the ordering wavevector along \hat{X} . The wavevector (H, K) for this order corresponds to $\mathbf{Q}_0 = (1/2, 0)$; reinstating the lattice units, this translates to $\mathbf{Q}_0 \simeq (0.628, 0)\text{\AA}^{-1}$. The dynamical spin correlations corresponding to this order show significant intensity at a band of excitations around an energy transfer $\hbar\omega \sim J_1^{XY}$. In addition, the Goldstone mode expected at \mathbf{Q}_0 for a simple XXZ model is gapped out by the anisotropy terms in the Hamiltonian, with a gap $\sim 0.3J_1^{XY}$. Below the scale of this Goldstone gap, we expect that the magnetic specific heat should be exponentially suppressed. Similar results follow for the exchange parameter set from Table IV.

On the other hand, experiments on $\text{BaCo}_2(\text{AsO}_4)_2$ and $\text{BaCo}_2(\text{PO}_4)_2$ do not find a zig-zag ordered ground state, but instead find a coplanar spiral order with a wavevector $(\mathbf{Q} \simeq (0.27, 0)$, or $(0.34, 0)\text{\AA}^{-1}$ for $\text{BaCo}_2(\text{AsO}_4)_2$ [33, 49]) and similar spiral order in $\text{BaCo}_2(\text{PO}_4)_2$ [32]. This suggests a slightly smaller third-neighbor coupling, reflecting the extreme sensitivity of the magnetic ground state to small changes in the frustration, which in turn might arise from small differences in the microscopic Kanamori interactions. To illustrate this, we have computed the magnetic ground state and dynamical spin correlations by rescaling the third-neighbor exchange interactions by a factor ≈ 0.61 , such that the renormalized $J_3^{XY}/J_1^{XY} = -0.3$. In this case, we find that the magnetic ground state has the experimentally reported ordering

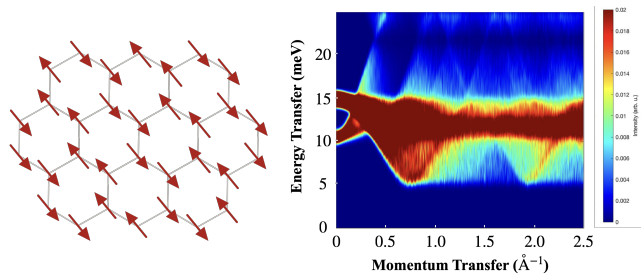


FIG. 7. Left panel: Zig-zag ordered phase with $\mathbf{Q}_0 = (1/2, 0) \approx (0.628, 0)\text{\AA}^{-1}$. Right panel: Powder averaged dynamical structure factor of the zig-zag ordered phase for the parameter set from Table III.

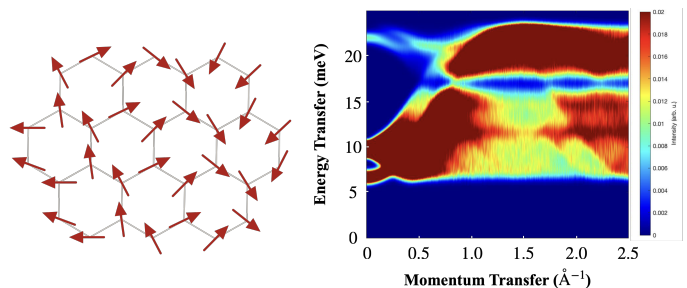


FIG. 8. Left panel: Spiral ordered phase with $\mathbf{Q}_0 = (0.34, 0)\text{\AA}^{-1}$. Right panel: Powder averaged dynamical structure factor of the zig-zag ordered phase for the parameter set from Table III but with all third-neighbor couplings rescaled such that $J_3^{XY}/J_1^{XY} = -0.3$.

wavevector, with the spin order as shown in Fig. 8 (left panel). The corresponding dynamical spin correlations are shown in Fig. 8 (right panel). As expected, the Goldstone mode continues to be gapped due to the anisotropic exchange terms. Indeed, inelastic neutron scattering experiments on $\text{BaCo}_2(\text{AsO}_4)_2$ and $\text{BaCo}_2(\text{PO}_4)_2$ find evidence for spin gapped excitations, qualitatively consistent with our results.

Specific heat measurements on $\text{BaCo}_2(\text{AsO}_4)_2$ have reported a $\sim T^2$ specific heat at very low temperature [33], which was attributed to 2D magnetic fluctuations. However, the spin gap seen in our calculations should strongly suppress the specific heat below a scale $\sim J_1^{XY}/3$; we thus conclude that the experimentally observed specific heat must be of non-magnetic origin. Alternatively, this might reflect the impact of disorder which has not been taken into account in our work.

One significant remaining discrepancy between our calculations and the experimental results on $\text{BaCo}_2(\text{AsO}_4)_2$ and $\text{BaCo}_2(\text{PO}_4)_2$ is in the overall scale of the magnetic exchange. The exchange couplings we find are about 3–4 times larger than those reported in the experimental literature. We have explored varying U, J_H and the crystal field matrix in order to resolve this discrepancy while maintaining a reasonable ratio of J_3^{XY}/J_1^{XY} , but without any success. We therefore suggest the following tentative explanation to reconcile this problem. We have seen that the Co^{2+} ion supports a lowest energy single-ion excitation, i.e. a spin exciton, at an energy $\simeq 20$ –30 meV. In CoTiO_3 , the exchange interactions between the $j = 1/2$ pseudospins is much smaller than this spin-exciton gap, justifying the restriction to a pseudospin-1/2 model. By contrast, the magnetic exchange interactions in $\text{BaCo}_2(\text{AsO}_4)_2$ and $\text{BaCo}_2(\text{PO}_4)_2$ are comparable to the spin-exciton gap. This suggests that the spin dynamics and Curie-Weiss temperatures might both be strongly impacted by coupling between the low energy magnon and the spin exciton. Level repulsion between these states could then lead to an effectively smaller magnon bandwidth for the $j = 1/2$ spins. We leave a more complete analysis of this magnon-exciton coupling to a future

publication.

VIII. CONCLUSION

We have explored the magnetism of the honeycomb cobaltates CoTiO_3 , $\text{BaCo}_2(\text{AsO}_4)_2$, and $\text{BaCo}_2(\text{PO}_4)_2$ which crystallize in the rhombohedral structure with $R\bar{3}$ space group. The Co^{2+} ions in the d^7 configuration have been proposed as possible candidate materials for realizing strong Kitaev interactions and Kitaev quantum spin liquids. Based on our combined DFT and exact diagonalization study, we find that the magnetism in these cobaltates is strongly perturbed by the trigonal distortion, and that they are better described as XXZ quantum magnets with subdominant but nevertheless important anisotropy terms. These anisotropy terms can gap the Goldstone modes in these magnets, and lead to a helical winding of the Dirac magnon nodal line in CoTiO_3 . In $\text{BaCo}_2(\text{AsO}_4)_2$ and $\text{BaCo}_2(\text{PO}_4)_2$, we have found microscopic evidence for strong third-neighbor antiferromagnetic exchange, which can drive possibly quite distinct quantum spin liquid phases. In addition, we have presented arguments that the low-energy spin excitations in the Ba compounds may involve strongly coupled magnons and spin excitons. While such magnon-exciton coupling has been previously explored within phenomenological models for CoTiO_3 [30] and FeI_2 [50], it would be worth extending those studies in order to provide a quantitative understanding of $\text{BaCo}_2(\text{AsO}_4)_2$ and $\text{BaCo}_2(\text{PO}_4)_2$, and their magnetic field driven phase diagram. Finally, while we have explored a limited set of all the honeycomb cobaltates, i.e. the rhombohedral examples, most other candidate cobaltates have even lower symmetry. For instance, $\text{Na}_3\text{Co}_2\text{SbO}_6$ [51–56],

$\text{Ag}_3\text{Co}_2\text{SbO}_6$ [57], $\text{Li}_3\text{Co}_2\text{SbO}_6$ [58, 59], and CoPS_3 [60] crystallize in the $C2/m$ space group, while $\text{Co}_4\text{Nb}_2\text{O}_9$ and $\text{Co}_4\text{Ta}_2\text{O}_9$ [61–64] crystallize in the $P\bar{3}c1$ space group. We thus suspect that they may support even more complex magnetic exchange interactions. In addition, the zig-zag magnetic order observed in many of these compounds may again stem from a significant third-neighbor coupling as was initially proposed also for the iridates [11] and also recognized to be important for the cobaltates by Liu and Khaliullin [25]. In other cobaltates, such as the recently studied $\text{Na}_2\text{Co}_2\text{TeO}_6$ [65] which crystallizes in the $P6_322$ space group and exhibits zig-zag magnetic order, randomness in the Na^+ arrangement might promote disorder-enabled spin liquid signatures. In summary, we argue that the honeycomb cobaltates can realize a rich set of magnetic Hamiltonians with frustration and anisotropic bond-dependent interactions. and may potentially host interesting quantum spin liquids driven by further-neighbor interactions and disorder. Realizing the Kitaev quantum spin liquid in this class of materials may require further fine-tuning of the chemistry and crystal fields in order to promote the Kitaev coupling over other competing exchange interactions.

ACKNOWLEDGMENTS

SV and AP thank Kate Ross for useful discussions, and acknowledge funding from NSERC of Canada. TS-D acknowledges J.C.Bose National Fellowship (grant no. JCB/2020/000004) for funding. SD was supported by a DST-INSPIRE fellowship. Exact diagonalization computations were performed on the Niagara supercomputer at the SciNet HPC Consortium. SciNet is funded by: the Canada Foundation for Innovation; the Government of Ontario; Ontario Research Fund - Research Excellence; and the University of Toronto.

-
- [1] Alexei Kitaev, “Anyons in an exactly solved model and beyond,” *Annals of Physics* **321**, 2–111 (2006), arXiv:0506438 [cond-mat].
 - [2] M. Hermanns, I. Kimchi, and J. Knolle, “Physics of the kitaev model: Fractionalization, dynamic correlations, and material connections,” *Annual Review of Condensed Matter Physics* **9**, 17–33 (2018), <https://doi.org/10.1146/annurev-conmatphys-033117-053934>.
 - [3] Hidenori Takagi, Tomohiro Takayama, George Jackeli, Giniyat Khaliullin, and Stephen E. Nagler, “Concept and realization of Kitaev quantum spin liquids,” (2019).
 - [4] Yukitoshi Motome, Ryoya Sano, Seonghoon Jang, Yusuke Sugita, and Yasuyuki Kato, “Materials design of Kitaev spin liquids beyond the Jackeli-Khaliullin mechanism,” *Journal of Physics Condensed Matter* **32**, 404001 (2020), arXiv:2001.03731.
 - [5] Jiri Chaloupka, George Jackeli, and Giniyat Khaliullin, “Kitaev-heisenberg model on a honeycomb lattice: Possible exotic phases in iridium oxides A_2IrO_3 ,” *Physical Review Letters* **105**, 027204 (2010), arXiv:1004.2964.
 - [6] Yoshihiko Okamoto, Minoru Nohara, Hiroko Aruga-Katori, and Hidenori Takagi, “Spin-liquid state in the $S=1/2$ hyperkagome antiferromagnet $\text{Na}_4\text{Ir}_3\text{O}_8$,” *Physical Review Letters* **99**, 137207 (2007), arXiv:0705.2821.
 - [7] Vamshi M. Katukuri, S. Nishimoto, V. Yushankhai, A. Stoyanova, H. Kandpal, Sungkyun Choi, R. Coldea, I. Rousochatzakis, L. Hozoi, and Jeroen Van Den Brink, “Kitaev interactions between $j = 1/2$ moments in honeycomb Na_2IrO_3 are large and ferromagnetic: Insights from ab initio quantum chemistry calculations,” *New Journal of Physics* **16**, 013056 (2014), arXiv:1312.7437.
 - [8] Jeffrey G. Rau, Eric Kin Ho Lee, and Hae Young Kee, “Generic spin model for the honeycomb iridates beyond the Kitaev limit,” *Physical Review Letters* **112**, 077204 (2014), arXiv:1310.7940.
 - [9] Yogesh Singh and P. Gegenwart, “Antiferromagnetic Mott insulating state in single crystals of the honeycomb lattice material Na_2IrO_3 ,” *Physical Review B - Condensed Matter and Materials Physics* **82**, 064412 (2010), arXiv:1006.0437.

- [10] S. K. Choi, R. Coldea, A. N. Kolmogorov, T. Lancaster, I. I. Mazin, S. J. Blundell, P. G. Radaelli, Yogesh Singh, P. Gegenwart, K. R. Choi, S. W. Cheong, P. J. Baker, C. Stock, and J. Taylor, “Spin waves and revised crystal structure of honeycomb iridate Na_2IrO_3 ,” *Physical Review Letters* **108**, 127204 (2012), arXiv:1202.1268.
- [11] Itamar Kimchi and Yi-Zhuang You, “Kitaev-heisenberg- J_2 - J_3 model for the iridates $A_2\text{IrO}_3$,” *Phys. Rev. B* **84**, 180407 (2011).
- [12] K. W. Plumb, J. P. Clancy, L. J. Sandilands, V. Vijay Shankar, Y. F. Hu, K. S. Burch, Hae Young Kee, and Young June Kim, “ α - RuCl_3 : A spin-orbit assisted Mott insulator on a honeycomb lattice,” *Physical Review B - Condensed Matter and Materials Physics* **90**, 041112 (2014), arXiv:1403.0883.
- [13] J. A. Sears, M. Songvilay, K. W. Plumb, J. P. Clancy, Y. Qiu, Y. Zhao, D. Parshall, and Young June Kim, “Magnetic order in α - RuCl_3 : A honeycomb-lattice quantum magnet with strong spin-orbit coupling,” *Physical Review B - Condensed Matter and Materials Physics* **91**, 144420 (2015), arXiv:1411.4610.
- [14] A. Banerjee, C. A. Bridges, J. Q. Yan, A. A. Aczel, L. Li, M. B. Stone, G. E. Granroth, M. D. Lumsden, R. Yiu, J. Knolle, S. Bhattacharjee, D. L. Kovrizhin, R. Moessner, D. A. Tennant, D. G. Mandrus, and S. E. Nagler, “Proximate Kitaev quantum spin liquid behaviour in a honeycomb magnet,” *Nature Materials* **15**, 733–740 (2016).
- [15] Daniel Weber, Leslie M. Schoop, Viola Duppel, Judith M. Lippmann, Jürgen Nuss, and Bettina V. Lotsch, “Magnetic Properties of Restacked 2D Spin 1/2 honeycomb RuCl_3 Nanosheets,” *Nano Letters* **16**, 3578–3584 (2016), arXiv:1603.04463.
- [16] Martin Grönke, Peer Schmidt, Martin Valldor, Steffen Oswald, Daniel Wolf, Axel Lubk, Bernd Büchner, and Silke Hampel, “Chemical vapor growth and delamination of α - RuCl_3 nanosheets down to the monolayer limit,” *Nanoscale* **10**, 19014–19022 (2018).
- [17] Soudabeh Mashhadi, Daniel Weber, Leslie M. Schoop, Armin Schulz, Bettina V. Lotsch, Marko Burghard, and Klaus Kern, “Electrical Transport Signature of the Magnetic Fluctuation-Structure Relation in α - RuCl_3 Nanoflakes,” *Nano Letters* **18**, 3203–3208 (2018).
- [18] Yingzhen Tian, Weiwei Gao, Erik A. Henriksen, James R. Chelikowsky, and Li Yang, “Optically Driven Magnetic Phase Transition of Monolayer RuCl_3 ,” *Nano Letters* **19**, 7673–7680 (2019).
- [19] Boyi Zhou, J. Balgley, P. Lampen-Kelley, J. Q. Yan, D. G. Mandrus, and E. A. Henriksen, “Evidence for charge transfer and proximate magnetism in graphene- α - RuCl_3 heterostructures,” *Physical Review B* **100**, 165426 (2019), arXiv:1811.04838.
- [20] Soudabeh Mashhadi, Youngwook Kim, Jeongwoo Kim, Daniel Weber, Takashi Taniguchi, Kenji Watanabe, Noejung Park, Bettina Lotsch, Jurgen H. Smet, Marko Burghard, and Klaus Kern, “Spin-Split Band Hybridization in Graphene Proximitized with α - RuCl_3 Nanosheets,” *Nano Letters* **19**, 4659–4665 (2019).
- [21] Sananda Biswas, Ying Li, Stephen M. Winter, Johannes Knolle, and Roser Valenti, “Electronic Properties of α - RuCl_3 in Proximity to Graphene,” *Physical Review Letters* **123**, 237201 (2019), arXiv:1908.04793.
- [22] Eli Gerber, Yuan Yao, Tomas A. Arias, and Eun Ah Kim, “Ab Initio Mismatched Interface Theory of Graphene on α - RuCl_3 : Doping and Magnetism,” *Physical Review Letters* **124**, 106804 (2020).
- [23] Y. Kasahara, K. Sugii, T. Ohnishi, M. Shimozawa, M. Yamashita, N. Kurita, H. Tanaka, J. Nasu, Y. Motome, T. Shibauchi, and Y. Matsuda, “Unusual Thermal Hall Effect in a Kitaev Spin Liquid Candidate α - RuCl_3 ,” *Physical Review Letters* **120**, 217205 (2018), arXiv:1709.10286.
- [24] Peter Czajka, Tong Gao, Max Hirschberger, Paula Lampen-Kelley, Arnab Banerjee, Jiaqiang Yan, David G. Mandrus, Stephen E. Nagler, and N. P. Ong, “Oscillations of the thermal conductivity in the spin-liquid state of α - RuCl_3 ,” *Nature Physics*, 1–5 (2021).
- [25] Huimei Liu and Giniyat Khaliullin, “Pseudospin exchange interactions in d7 cobalt compounds: Possible realization of the Kitaev model,” *Physical Review B* **97**, 014407 (2018), arXiv:1710.10193.
- [26] Huimei Liu, Jiri Chaloupka, and Giniyat Khaliullin, “Kitaev Spin Liquid in 3d Transition Metal Compounds,” *Physical Review Letters* **125**, 47201 (2020), arXiv:2002.05441.
- [27] Stephen M. Winter, Ying Li, Harald O. Jeschke, and Roser Valenti, “Challenges in design of kitaev materials: Magnetic interactions from competing energy scales,” *Phys. Rev. B* **93**, 214431 (2016).
- [28] Ruidan Zhong, Tong Gao, Nai Phuan Ong, and Robert J. Cava, “Weak-field induced nonmagnetic state in a Co-based honeycomb,” arXiv, 1–8 (2019).
- [29] Bo Yuan, Ilia Khait, Guo Jiun Shu, F. C. Chou, M. B. Stone, J. P. Clancy, Arun Paramakanti, and Young June Kim, “Dirac Magnons in a Honeycomb Lattice Quantum XY Magnet CoTiO_3 ,” *Physical Review X* **10**, 011062 (2020), arXiv:1907.02061.
- [30] M. Elliot, P. A. McClarty, D. Prabhakaran, R. D. Johnson, H. C. Walker, P. Manuel, and Radu Coldea, “Visualization of isospin momentum texture of dirac magnons and excitons in a honeycomb quantum magnet,” arXiv, 1–28 (2020), arXiv:2007.04199.
- [31] J. B. Fouet, P. Sindzingre, C. Lhuillier, “An investigation of the quantum J_1 - J_2 - J_3 model on the honeycomb lattice,” *the European Physical Journal B* **162**, 147–162 (2004).
- [32] Harikrishnan S. Nair, J. M. Brown, E. Coldren, G. Hester, M. P. Gelfand, A. Podlesnyak, Q. Huang, and K. A. Ross, “Short-range order in the quantum XXZ honeycomb lattice material $\text{BaCo}_2(\text{PO}_4)_2$,” *Physical Review B* **97**, 134409 (2018), arXiv:1712.06208.
- [33] L. P. Regnault, C. Boullier, and J. E. Lorenzo, “Polarized-neutron investigation of magnetic ordering and spin dynamics in $\text{BaCo}_2(\text{AsO}_4)_2$ frustrated honeycomb-lattice magnet,” *Heliyon* **4**, 1–37 (2018), arXiv:1801.06588.
- [34] John P. Perdew, J. A. Chevary, S. H. Vosko, Koblar A. Jackson, Mark R. Pederson, D. J. Singh, and Carlos Fiolhais, “Atoms, molecules, solids, and surfaces: Applications of the generalized gradient approximation for exchange and correlation,” *Phys. Rev. B* **46**, 6671–6687 (1992).
- [35] See Supplemental Material online.
- [36] G. Kresse and J. Furthmüller, “Efficient iterative schemes for ab initio total-energy calculations using a plane-wave basis set,” *Phys. Rev. B* **54**, 11169–11186 (1996).
- [37] P. E. Blöchl, “Projector augmented-wave method,” *Phys. Rev. B* **50**, 17953–17979 (1994).

- [38] John P. Perdew, Kieron Burke, and Matthias Ernzerhof, “Generalized gradient approximation made simple,” *Phys. Rev. Lett.* **77**, 3865–3868 (1996).
- [39] A. I. Liechtenstein, V. I. Anisimov, and J. Zaanen, “Density-functional theory and strong interactions: Orbital ordering in mott-hubbard insulators,” *Phys. Rev. B* **52**, R5467–R5470 (1995).
- [40] Lei Wang, Thomas Maxisch, and Gerbrand Ceder, “Oxidation energies of transition metal oxides within the GGA + U framework,” *Phys. Rev. B* **73**, 195107 (2006).
- [41] Marçal Capdevila-Cortada, Zbigniew Lodziana, and Nuria Lopez, “Performance of dft+u approaches in the study of catalytic materials,” *ACS Catalysis* **6**, 8370–8379 (2016), <https://doi.org/10.1021/acscatal.6b01907>.
- [42] O. K. Andersen and T. Saha-Dasgupta, “Muffin-tin orbitals of arbitrary order,” *Phys. Rev. B* **62**, R16219–R16222 (2000).
- [43] O. K. Andersen and O. Jepsen, “Explicit, first-principles tight-binding theory,” *Phys. Rev. Lett.* **53**, 2571–2574 (1984).
- [44] Antoine Georges, Luca De Medici, and Jernej Mravlje, “Strong correlations from hund’s coupling,” *Annual Review of Condensed Matter Physics* **4**, 137–178 (2013).
- [45] Sadamichi Maekawa, Takami Tohyama, Stewart E. Barnes, Sumio Ishihara, Wataru Koshibae, and Giniyat Khaliullin, *Physics of Transition Metal Oxides*, Springer Series in Solid-State Sciences, Vol. 144 (Springer Berlin Heidelberg, Berlin, Heidelberg, 2004).
- [46] LJ de Jongh, “Magnetic Properties of Layered TMOs,” *Journal of Chemical Information and Modeling* **53**, 1689–1699 (2013), arXiv:arXiv:1011.1669v3.
- [47] K. A. Ross, J. M. Brown, R. J. Cava, J. W. Krizan, S. E. Nagler, J. A. Rodriguez-Rivera, and M. B. Stone, “Single-ion properties of the $S_{\text{eff}} = \frac{1}{2}$ xy antiferromagnetic pyrochlores $\text{Na}_3\text{A}'\text{Co}_2\text{F}_7$ ($\text{A}' = \text{Ca}^{2+}, \text{Sr}^{2+}$),” *Phys. Rev. B* **95**, 144414 (2017).
- [48] S. Toth and B. Lake, “Linear spin wave theory for single-Q incommensurate magnetic structures,” *Journal of Physics Condensed Matter* **27** (2014), 10.1088/0953-8984/27/16/166002, arXiv:1402.6069.
- [49] L. P. Regnault, P. Burlet, and J. Rossat-Mignod, “Magnetic ordering in a planar X - Y model: $\text{BaCo}_2(\text{AsO}_4)_2$,” *Physica B+C* **86-88**, 660–662 (1977).
- [50] Xiaojian Bai, Shang Shun Zhang, Zhiling Dun, Hao Zhang, Qing Huang, Haidong Zhou, Matthew B. Stone, Alexander I. Kolesnikov, Feng Ye, Cristian D. Batista, and Martin Mourigal, “Hybridized quadrupolar excitations in the spin-anisotropic frustrated magnet Fe_2 ,” *Nature Physics* **17**, 467–472 (2021), arXiv:2004.05623.
- [51] L. Viciu, Q. Huang, E. Morosan, HW Zandbergen, Ni Greenbaum, T McQueen, and R.J Cava, “Structure and basic magnetic properties of the honeycomb lattice compounds,” *Journal of Solid State Chemistry* **180**, 1060–1067 (2007).
- [52] M. Songvilay, J. Robert, S. Petit, J. A. Rodriguez-Rivera, W. D. Ratcliff, F. Damay, V. Balédent, M. Jiménez-Ruiz, P. Lejay, E. Pachoud, A. Hadj-Azzem, V. Simonet, and C. Stock, “Kitaev interactions in the Co honeycomb antiferromagnets $\text{Na}_3\text{Co}_2\text{SbO}_6$ and $\text{Na}_2\text{Co}_2\text{TeO}_6$,” *Physical Review B* **102**, 224429 (2020), arXiv:2012.00006.
- [53] E. Lefrançois, M. Songvilay, J. Robert, G. Nataf, E. Jordan, L. Chaix, C. V. Colin, P. Lejay, A. Hadj-Azzem, R. Ballou, and V. Simonet, “Magnetic properties of the honeycomb oxide $\text{Na}_2\text{Co}_2\text{TeO}_6$,” *Physical Review B* **94**, 214416 (2016), arXiv:1608.07593.
- [54] Guiling Xiao, Zhengcai Xia, Wanwan Zhang, Xiaoyu Yue, Sha Huang, Xiaoxing Zhang, Feng Yang, Yujie Song, Meng Wei, Han Deng, and Dequan Jiang, “Crystal Growth and the Magnetic Properties of $\text{Na}_2\text{Co}_2\text{TeO}_6$ with Quasi-Two-Dimensional Honeycomb Lattice,” *Crystal Growth and Design* **19**, 2568–2662 (2019).
- [55] A. K. Bera, S. M. Yusuf, Amit Kumar, and C. Ritter, “Zigzag antiferromagnetic ground state with anisotropic correlation lengths in the quasi-two-dimensional honeycomb lattice compound $\text{Na}_2\text{Co}_2\text{TeO}_6$,” *Physical Review B* **95**, 094424 (2017).
- [56] Cheryl Wong, Maxim Avdeev, and Chris D. Ling, “Zig-zag magnetic ordering in honeycomb-layered $\text{Na}_3\text{Co}_2\text{SbO}_6$,” *Journal of Solid State Chemistry* **243**, 18–22 (2016).
- [57] E. A. Zvereva, M. I. Stratan, A. V. Ushakov, V. B. Nalbandyan, I. L. Shukaev, A. V. Silhanek, M. Abdel-Hafez, S. V. Streltsov, and A. N. Vasiliev, “Orbitally induced hierarchy of exchange interactions in the zigzag antiferromagnetic state of honeycomb silver delafossite $\text{Ag}_3\text{Co}_2\text{SbO}_6$,” *Dalton Transactions* **45**, 7373–7384 (2016).
- [58] Alex J. Brown, Qingbo Xia, Maxim Avdeev, Brendan J. Kennedy, and Chris D. Ling, “Synthesis-Controlled Polymorphism and Magnetic and Electrochemical Properties of $\text{Li}_3\text{Co}_2\text{SbO}_6$,” *Inorganic Chemistry* **58**, 13881–13891 (2019).
- [59] Mikhail I. Stratan, Igor L. Shukaev, Tatyana M. Vasilchikova, Alexander N. Vasiliev, Artem N. Korshunov, Alexander I. Kurbakov, Vladimir B. Nalbandyan, and Elena A. Zvereva, “Synthesis, structure and magnetic properties of honeycomb-layered $\text{Li}_3\text{Co}_2\text{SbO}_6$ with new data on its sodium precursor, $\text{Na}_3\text{Co}_2\text{SbO}_6$,” *New Journal of Chemistry* **43**, 13545–13553 (2019).
- [60] A. R. Wildes, V. Simonet, E. Ressouche, R. Ballou, and G. J. McIntyre, “The magnetic properties and structure of the quasi-two-dimensional antiferromagnet CoPS_3 ,” *Journal of Physics Condensed Matter* **29**, 455801 (2017), arXiv:1706.07989.
- [61] E. F. Bertaut, L. Corliss, F. Forrat, R. Aleonard, and R. Pauthenet, “Etude de niobates et tantalates de métaux de transition bivalents,” *Journal of Physics and Chemistry of Solids* **21**, 234–251 (1961).
- [62] N. D. Khanh, N. Abe, H. Sagayama, A. Nakao, T. Hanashima, R. Kiyonagi, Y. Tokunaga, and T. Arima, “Magnetoelectric coupling in the honeycomb antiferromagnet $\text{Co}_4\text{Nb}_2\text{O}_9$,” *Physical Review B* **93**, 075117 (2016).
- [63] Yuki Yanagi, Satoru Hayami, and Hiroaki Kusunose, “Manipulating the magnetoelectric effect: Essence learned from $\text{Co}_4\text{Nb}_2\text{O}_9$,” *Physical Review B* **97**, 020404 (2018).
- [64] Yuki Yanagi, Satoru Hayami, and Hiroaki Kusunose, “Theory of magnetoelectric response in $\text{Co}_4\text{Nb}_2\text{O}_9$,” *Physica B: Condensed Matter* **536**, 107–110 (2018).
- [65] Anjana M. Samarakoon, Qiang Chen, Haidong Zhou, and V. Ovidiu Garlea, “Static and dynamic magnetic properties of honeycomb lattice antiferromagnets $\text{na}_2\text{m}_2\text{teo}_6$, $m = \text{co}$ and ni ,” (2021), arXiv:2105.06549 [cond-mat.str-el].

Appendix A: Exchange couplings in local Kitaev basis

In this Appendix, we discuss the basis rotation and the rewriting of the exchange couplings in the Kitaev basis. The spins written in the global XYZ basis (\mathcal{S}_α) can be transformed into the local $\tilde{x}\tilde{y}\tilde{z}$ basis ($\tilde{\mathcal{S}}_\alpha$) via a transformation $\tilde{\mathcal{S}}_\alpha = \mathcal{U}_{\alpha\beta}\mathcal{S}_\beta$, where \mathcal{U} is given by the matrix

$$\mathcal{U} = \begin{pmatrix} 1/\sqrt{6} & 1/\sqrt{2} & 1/\sqrt{3} \\ -\sqrt{2}/3 & 0 & 1/\sqrt{3} \\ 1/\sqrt{6} & -1/\sqrt{2} & 1/\sqrt{3} \end{pmatrix} \quad (\text{A1})$$

Thus, the local exchange matrix \mathcal{J}_{loc} is obtained via

$$\mathcal{J}_{\text{loc}} = \mathcal{U}\mathcal{J}\mathcal{U}^T \quad (\text{A2})$$

where \mathcal{J} is the exchange matrix in the global basis. Along the same C bond (referred to in the local basis as the z bond), the Heisenberg (J), Kitaev (K), Diagonal (η) and off-diagonal (Γ , Γ'_1 , Γ'_2) anisotropy couplings are defined as

$$\mathcal{J}_{\text{loc}}^{(z)} = \begin{pmatrix} J + \eta & \Gamma & \Gamma'_1 \\ \Gamma & J - \eta & \Gamma'_2 \\ \Gamma'_1 & \Gamma'_2 & J + K \end{pmatrix} \quad (\text{A3})$$

Below we present the couplings in this local basis for the materials considered. It should be noted that many couplings have comparable values, which does not allow for as simple a description as the XXZ model in the global basis which is presented in the main text.

CoTiO_3	Bond-1	Bond-1'	Bond-2'
J	-3.80	0.33	1.07
K	1.37	0	0.12
Γ	2.08	0	-0.17
η	-1.84	0	0
Γ'_1	-0.57	0	-0.18
Γ'_2	2.73	0	-0.35

TABLE V. Local exchange couplings for CoTiO_3 .

$\text{BaCo}_2(\text{AsO}_4)_2$	Bond-1	Bond-3
J	-12.40	5.51
K	2.06	-0.30
Γ	4.05	-1.44
η	-0.84	0.00
Γ'_1	1.82	-1.42
Γ'_2	4.89	-1.45

TABLE VI. Local exchange couplings for $\text{BaCo}_2(\text{AsO}_4)_2$.

$\text{BaCo}_2(\text{PO}_4)_2$	Bond-1	Bond-3
J	-13.04	5.21
K	-3.11	-0.05
Γ	2.00	-1.05
η	-1.35	0.00
Γ'_1	6.41	-1.45
Γ'_2	3.38	-1.24

TABLE VII. Local exchange couplings for $\text{BaCo}_2(\text{PO}_4)_2$.

Appendix B: J_1 - J_2 - J_3 Phase Diagram

The figure below shows the classical J_1 - J_2 - J_3 phase diagram explored in [31]. In this work, we find that the relevant part of the phase diagram is the y -axis, specifically where $J_3/J_1 < 0$. Experiments on the Barium compounds appear to stabilize the shaded "Spiral 2" phase (characterized by a nonzero angle between spins on different sublattices). While the aforementioned study does not consider off-diagonal anisotropy terms (D and E), we find that including them retains the general structure of the phase diagram. The narrowness of this spiral phase emphasizes the sensitivity of the magnetic order to the microscopics of the systems considered.

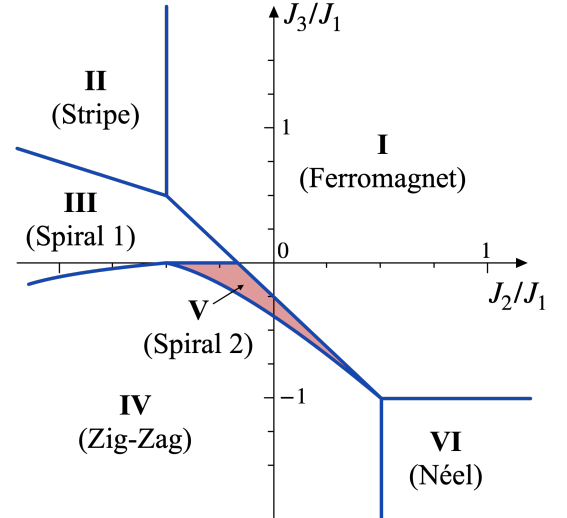


FIG. 9. Classical phase diagram for the J_1 - J_2 - J_3 model, reproduced from [31]

SUPPLEMENTARY MATERIAL

Can we realize Kitaev quantum spin liquids in the $j_{\text{eff}} = 1/2$ honeycomb cobaltates?

Shreya Das,^{1,*} Sreekar Voleti,^{2,*} Tanusri Saha-Dasgupta,^{1,†} and Arun Paramekanti^{2,‡}

¹*Department of Condensed Matter Physics and Materials Science,
S.N. Bose National Centre for Basic Sciences, Kolkata 700098, India.*

²*Department of Physics, University of Toronto, Toronto, Ontario, M5S 1A7, Canada*

arXiv:2106.11982v1 [cond-mat.str-el] 22 Jun 2021

* These authors contributed equally

† tanusri@bose.res.in

‡ arunp@physics.utoronto.ca

I. DFT CALCULATION DETAILS

We carried out theoretical calculations within the framework of first-principles density functional theory (DFT) taking into account the structural as well as chemical information completely.

Our DFT based calculations were executed with the choices of different basis sets as, (i) the plane-wave based basis as implemented in the Vienna *ab-initio* Simulation Package (VASP) [1] with projector-augmented wave (PAW) potential [] and (ii) the muffin-tin orbital (MTO) based linear muffin-tin orbital (LMTO) method [2], and the N^{th} order MTO method namely, NMTO method [3], as implemented in the STUTTGART code.

The consistency of results between two different basis sets have been confirmed in terms density of states, band structure and magnetic moments. The exchange correlation functional was chosen as the generalized gradient approximation (GGA) implemented following the Perdew-Burke-Ernzerhof (PBE) prescription [4].

For the plane wave calculation, energy cutoff of 600 eV and MonkhorstPack k-points mesh of $6 \times 6 \times 2$ for the unit cell of CoTiO_3 and $\text{BaCo}_2(\text{AsO}_4)_2$ were found to provide good convergence of the total energy in self-consistent field calculations. The effect of spin-orbit coupling (SOC) was included within GGA+SOC implementation of VASP and the effect of missing correlation effect beyond GGA at the Co site was considered within the GGA+SOC+U framework [5] with the choice of $U = 3$ eV and Hund's coupling $J_H = 0.7$ eV [6, 7].

For construction of low energy Hamiltonian, we used the N^{th} order muffin-tin orbital method, which relies on a self-consistent potential generated by the linear MTO (LMTO) method. The low-energy tight-binding Hamiltonian, defined in the effective Co Wannier basis, provides information about the crystal-field splitting at the Co site along with the effective hopping interactions between the Co sites. The muffin-tin radii of different atomic sites used in LMTO calculations were chosen as 1.52 Å for Co, 1.27 Å for Ti, 0.98 Å for O atoms in CoTiO_3 ; 2.44 Å for Ba, 1.52 Å for Co, 1.09 Å for As and 0.82/0.89 Å for the O atoms in $\text{BaCo}_2(\text{AsO}_4)_2$. For $\text{BaCo}_2(\text{PO}_4)_2$, the atomic radii are chosen to be 2.43 Å for Ba, 1.58 Å for Co, 0.97 Å for P and 0.74/0.83 Å for the O atoms.

II. ONSITE MATRICES

The on-site term (H_{CF}) is written in second quantized language as

$$H_{\text{CF}} = \sum_{\ell\ell'} A_{\ell m} \sum_s c_{\ell s}^\dagger c_{ms}$$

where ℓ and m are orbital indices, and s refers to the electron spin. Below, we present the A matrices for each of the materials considered in the main text. All the matrices below are written in the orbital basis $\{(yz, xz, xy), (x^2 - y^2, 3z^2 - 1)\}$

A. CoTiO_3

$$A_{\text{CTO}} = \begin{pmatrix} -1.1642 & 0.0312 & -0.0008 & -0.0063 & -0.0039 \\ 0.0312 & -0.1429 & -0.0040 & 0.0033 & -0.0044 \\ -0.0008 & -0.004 & -1.0968 & 0.0926 & 0.0103 \\ -0.0063 & 0.0033 & 0.0926 & -0.4133 & 0.4380 \\ -0.0039 & -0.0044 & 0.0103 & 0.4380 & -0.8765 \end{pmatrix} \quad (1)$$

B. $\text{BaCo}_2(\text{AsO}_4)_2$

$$A_{\text{BCAO}} = \begin{pmatrix} -2.9578 & 0.0140 & -0.0005 & 0.0202 & 0.0123 \\ 0.0140 & -1.6838 & 0.0124 & 0.0020 & -0.0043 \\ -0.0005 & 0.0124 & -2.8610 & 0.049 & -0.0495 \\ 0.0202 & 0.0020 & 0.0490 & -1.9904 & 0.5312 \\ 0.0123 & -0.0043 & -0.04950 & 0.5312 & -2.6055 \end{pmatrix} \quad (2)$$

C. BaCo₂(PO₄)₂

$$A_{\text{BCPO}} = \begin{pmatrix} -3.5049 & -0.0717 & 0.0008 & 0.0034 & 0.0008 \\ -0.0717 & -2.2912 & 0.0017 & -0.0136 & 0.0249 \\ 0.0008 & 0.0017 & -3.4155 & -0.0900 & 0.0157 \\ 0.0034 & -0.0136 & -0.0900 & -2.5757 & 0.5051 \\ 0.0008 & 0.0249 & 0.0157 & 0.5051 & -3.186 \end{pmatrix} \quad (3)$$

III. HOPPING MATRICES

Below, we list the hopping matrices for the relevant bonds, listing both the connecting vector \vec{V} , as well as the associated hopping matrix T . These should be read in terms of the hopping Hamiltonian (in the same basis as above)

$$\hat{T}_{i,i+\vec{V}} = \sum_{\ell\ell'\alpha} (T_{\ell\ell'} c_{i+\vec{V},\ell'\alpha}^\dagger c_{i\ell\alpha} + T_{\ell'\ell}^t c_{i\ell\alpha}^\dagger c_{i+\vec{V},\ell'\alpha}) \quad (4)$$

A. CoTiO₃

1. In-plane 1st Nearest Neighbour

$$\vec{V} = (-0.5, -0.866, 0.205) \quad , \quad T = \begin{pmatrix} -0.0803 & -0.0411 & 0.1233 & -0.0163 & -0.0415 \\ -0.0411 & -0.0588 & 0.0236 & -0.0143 & -0.0433 \\ 0.1233 & 0.0236 & -0.0684 & 0.0575 & -0.0073 \\ -0.0163 & -0.0143 & 0.0575 & -0.0333 & -0.0641 \\ -0.0415 & -0.0433 & -0.0073 & -0.0641 & -0.0093 \end{pmatrix} \quad (5)$$

$$\vec{V} = (1.0, 0.0, 0.205) \quad , \quad T = \begin{pmatrix} 0.0012 & -0.0100 & -0.0026 & -0.0243 & -0.0134 \\ -0.0100 & -0.0427 & 0.0194 & 0.0268 & -0.0026 \\ -0.0026 & 0.0194 & 0.0793 & -0.0515 & -0.0051 \\ -0.0243 & 0.0268 & -0.0515 & -0.1734 & 0.0811 \\ -0.0134 & -0.0026 & -0.0051 & 0.0811 & -0.1146 \end{pmatrix} \quad (6)$$

$$\vec{V} = (-0.5, 0.866, 0.205) \quad , \quad T = \begin{pmatrix} -0.0779 & -0.0214 & -0.1259 & -0.0006 & 0.0287 \\ -0.0214 & -0.0991 & -0.0691 & 0.0119 & 0.0123 \\ -0.1259 & -0.0691 & -0.0744 & 0.0405 & -0.0154 \\ -0.0006 & 0.0119 & 0.0405 & -0.0364 & -0.0271 \\ 0.0287 & 0.0123 & -0.0154 & -0.0271 & 0.0376 \end{pmatrix} \quad (7)$$

2. Out-of-plane 1st Nearest Neighbour

$$\vec{V} = (0.0, 0.0, 1.381) \quad , \quad T = \begin{pmatrix} -0.0015 & 0.0210 & 0.0010 & 0.0082 & 0.0052 \\ 0.0210 & 0.027 & 0.0052 & -0.0049 & 0.0067 \\ 0.0010 & 0.0052 & -0.019 & -0.0097 & 0.0033 \\ 0.0082 & -0.0049 & -0.0097 & 0.0353 & 0.0086 \\ 0.0052 & 0.0067 & 0.0033 & 0.0086 & -0.0142 \end{pmatrix} \quad (8)$$

3. *Out-of-plane 2nd Nearest Neighbour*

$$\vec{V} = (-0.5, -0.866, 1.587) \quad , \quad T = \begin{pmatrix} -0.0089 & -0.0308 & -0.0046 & -0.0155 & 0.0042 \\ 0.0358 & 0.0038 & 0.0106 & 0.0063 & -0.0129 \\ 0.0131 & 0.0124 & 0.0070 & 0.0079 & -0.0065 \\ 0.0208 & 0.0234 & -0.0049 & 0.0144 & -0.0140 \\ 0.0005 & 0.0276 & -0.0167 & 0.0264 & -0.0216 \end{pmatrix} \quad (9)$$

$$\vec{V} = (0.5, 0.866, -1.587) \quad , \quad T = \begin{pmatrix} -0.0089 & 0.0358 & 0.0131 & 0.0208 & 0.0005 \\ -0.0308 & 0.0038 & 0.0124 & 0.0234 & 0.0276 \\ -0.0046 & 0.0106 & 0.0070 & -0.0049 & -0.0167 \\ -0.0155 & 0.0063 & 0.0079 & 0.0144 & 0.0264 \\ 0.0042 & -0.0129 & -0.0065 & -0.0140 & -0.0216 \end{pmatrix} \quad (10)$$

$$\vec{V} = (1.0, 0.0, 1.587) \quad , \quad T = \begin{pmatrix} 0.0109 & -0.0542 & 0.0071 & -0.0099 & -0.0169 \\ 0.0275 & 0.0071 & 0.0056 & -0.0019 & -0.0022 \\ -0.0295 & 0.0188 & -0.0137 & 0.0062 & 0.0201 \\ -0.0036 & -0.0051 & -0.0085 & 0.0013 & 0.0184 \\ 0.0104 & -0.0117 & 0.0016 & 0.0017 & -0.0109 \end{pmatrix} \quad (11)$$

$$\vec{V} = (-1.0, 0.0, -1.587) \quad , \quad T = \begin{pmatrix} 0.0109 & 0.0275 & -0.0295 & -0.0036 & 0.0104 \\ -0.0542 & 0.0071 & 0.0188 & -0.0051 & -0.0117 \\ 0.0071 & 0.0056 & -0.0137 & -0.0085 & 0.0016 \\ -0.0099 & -0.0019 & 0.0062 & 0.0013 & 0.0017 \\ -0.0169 & -0.0022 & 0.0201 & 0.0184 & -0.0109 \end{pmatrix} \quad (12)$$

$$\vec{V} = (-0.5, 0.866, 1.587) \quad , \quad T = \begin{pmatrix} 0.0174 & -0.0180 & 0.0049 & -0.0224 & 0.0102 \\ 0.0232 & -0.0098 & 0.0085 & -0.0022 & 0.0031 \\ -0.0146 & -0.0278 & 0.0052 & 0.0079 & -0.0013 \\ 0.0534 & 0.0160 & 0.0090 & -0.0153 & 0.0179 \\ 0.0093 & -0.0087 & 0.0063 & 0.0024 & -0.0027 \end{pmatrix} \quad (13)$$

$$\vec{V} = (0.5, -0.866, -1.587) \quad , \quad T = \begin{pmatrix} 0.0174 & 0.0232 & -0.0146 & 0.0534 & 0.0093 \\ -0.0180 & -0.0098 & -0.0278 & 0.0160 & -0.0087 \\ 0.0049 & 0.0085 & 0.0052 & 0.0090 & 0.0063 \\ -0.0224 & -0.0022 & 0.0079 & -0.0153 & 0.0024 \\ 0.0102 & 0.0031 & -0.0013 & 0.0179 & -0.0027 \end{pmatrix} \quad (14)$$

B. $\text{BaCo}_2(\text{AsO}_4)_2$ 1. *In-plane 1st Nearest Neighbour*

$$\vec{V} = (-0.5, -0.866, 0.056) \quad , \quad T = \begin{pmatrix} -0.1539 & -0.0133 & 0.1892 & -0.0808 & 0.0095 \\ -0.0133 & -0.0250 & 0.0676 & -0.0087 & 0.0115 \\ 0.1892 & 0.0676 & -0.0883 & 0.0240 & -0.0012 \\ -0.0808 & -0.0087 & 0.0240 & 0.0292 & -0.056 \\ 0.0095 & 0.0115 & -0.0012 & -0.056 & 0.0176 \end{pmatrix} \quad (15)$$

$$\vec{V} = (1.0, 0.0, 0.056) \quad , \quad T = \begin{pmatrix} 0.0961 & 0.0558 & 0.0009 & 0.0123 & -0.0033 \\ 0.0558 & -0.0240 & -0.0076 & 0.0129 & -0.0221 \\ 0.0009 & -0.0076 & 0.0442 & 0.0052 & -0.0476 \\ 0.0123 & 0.0129 & 0.0052 & -0.1668 & 0.1650 \\ -0.0033 & -0.0221 & -0.0476 & 0.1650 & -0.1699 \end{pmatrix} \quad (16)$$

$$\vec{V} = (-0.5, 0.866, 0.056) \quad , \quad T = \begin{pmatrix} -0.1581 & -0.0391 & -0.1913 & 0.0531 & -0.0147 \\ -0.0391 & -0.0226 & -0.0711 & 0.0043 & -0.0034 \\ -0.1913 & -0.0711 & -0.0849 & 0.0005 & -0.0034 \\ 0.0531 & 0.0043 & 0.0005 & 0.0416 & -0.0649 \\ -0.0147 & -0.0034 & -0.0034 & -0.0649 & 0.0038 \end{pmatrix} \quad (17)$$

2. In-plane 3rd Nearest Neighbour

$$\vec{V} = (1.0, 1.732, 0.056) \quad , \quad T = \begin{pmatrix} -0.0177 & -0.0075 & 0.0255 & -0.0102 & -0.0026 \\ -0.0075 & 0.0013 & 0.0298 & -0.0658 & -0.0377 \\ 0.0255 & 0.0298 & -0.0283 & -0.0060 & -0.0005 \\ -0.0102 & -0.0658 & -0.0060 & 0.0653 & 0.0394 \\ -0.0026 & -0.0377 & -0.0005 & 0.0394 & 0.0251 \end{pmatrix} \quad (18)$$

$$\vec{V} = (-2.0, 0.0, 0.056) \quad , \quad T = \begin{pmatrix} 0.0061 & 0.0137 & -0.0007 & 0.0077 & 0.0000 \\ 0.0137 & 0.1327 & -0.0134 & -0.0042 & 0.0078 \\ -0.0007 & -0.0134 & -0.0027 & -0.0086 & 0.0015 \\ 0.0077 & -0.0042 & -0.0086 & -0.0646 & 0.0149 \\ 0.0000 & 0.0078 & 0.0015 & 0.0149 & -0.0258 \end{pmatrix} \quad (19)$$

$$\vec{V} = (1.0, -1.732, 0.056) \quad , \quad T = \begin{pmatrix} -0.0226 & -0.0107 & -0.0243 & 0.0141 & 0.0094 \\ -0.0107 & 0.0019 & -0.0084 & 0.0661 & 0.0363 \\ -0.0243 & -0.0084 & -0.0242 & 0.0129 & 0.0151 \\ 0.0141 & 0.0661 & 0.0129 & 0.0856 & 0.0260 \\ 0.0094 & 0.0363 & 0.0151 & 0.0260 & 0.0051 \end{pmatrix} \quad (20)$$

C. BaCo₂(PO₄)₂

1. In-plane 1st Nearest Neighbour

$$\vec{V} = (-0.5, -0.866, 0.059) \quad , \quad T = \begin{pmatrix} 0.1162 & -0.0458 & 0.0024 & -0.0152 & 0.0031 \\ -0.0458 & -0.0748 & 0.0106 & 0.0078 & -0.0217 \\ 0.0024 & 0.0106 & 0.0363 & 0.0057 & 0.0519 \\ -0.0152 & 0.0078 & 0.0057 & -0.1642 & 0.1553 \\ 0.0031 & -0.0216 & 0.0519 & 0.1553 & -0.2813 \end{pmatrix} \quad (21)$$

$$\vec{V} = (1.0, 0.0, 0.059) \quad , \quad T = \begin{pmatrix} -0.2091 & 0.0040 & -0.2255 & -0.0496 & 0.0435 \\ 0.0040 & -0.0612 & 0.0309 & 0.0033 & -0.0031 \\ -0.2255 & 0.0309 & -0.0987 & 0.0137 & 0.0194 \\ -0.0496 & 0.0033 & 0.0137 & 0.0115 & -0.0874 \\ 0.0435 & -0.0031 & 0.0194 & -0.0874 & -0.0103 \end{pmatrix} \quad (22)$$

$$\vec{V} = (-0.5, 0.866, 0.059) \quad , \quad T = \begin{pmatrix} -0.1827 & -0.0309 & 0.2215 & 0.0908 & -0.0315 \\ -0.0309 & -0.0711 & -0.0265 & 0.0043 & 0.0059 \\ 0.2215 & -0.0265 & -0.1217 & -0.0213 & 0.0096 \\ 0.0908 & 0.0043 & -0.0213 & -0.0084 & -0.0761 \\ -0.0315 & 0.0059 & 0.0096 & -0.0761 & 0.0161 \end{pmatrix} \quad (23)$$

2. In-plane 3rd Nearest Neighbour

$$\vec{V} = (1.0, 1.732, 0.056) \quad , \quad T = \begin{pmatrix} 0.0243 & -0.0360 & -0.0014 & -0.0084 & -0.0044 \\ -0.0360 & 0.1278 & 0.0189 & -0.0055 & 0.0141 \\ -0.0014 & 0.0189 & -0.0197 & 0.0236 & -0.0042 \\ -0.0084 & -0.0055 & 0.0236 & -0.0463 & 0.0087 \\ -0.0044 & 0.0141 & -0.0042 & 0.0087 & -0.0275 \end{pmatrix} \quad (24)$$

$$\vec{V} = (-2.0, 0.0, 0.056) \quad , \quad T = \begin{pmatrix} -0.0118 & -0.0024 & -0.0208 & -0.0211 & -0.0054 \\ -0.0024 & 0.0038 & 0.0056 & 0.0639 & 0.0348 \\ -0.0208 & 0.0056 & -0.0276 & -0.0066 & -0.0233 \\ -0.0211 & 0.0639 & -0.0066 & 0.1013 & 0.0172 \\ -0.0054 & 0.0348 & -0.0233 & 0.0172 & -0.0072 \end{pmatrix} \quad (25)$$

$$\vec{V} = (1.0, -1.732, 0.056) \quad , \quad T = \begin{pmatrix} -0.0062 & -0.0117 & 0.0222 & 0.0200 & 0.0014 \\ -0.0117 & 0.0059 & -0.0292 & -0.0659 & -0.0358 \\ 0.0222 & -0.0292 & -0.0342 & 0.0151 & -0.0116 \\ 0.0200 & -0.0659 & 0.0151 & 0.0809 & 0.0298 \\ 0.0014 & -0.0358 & -0.0116 & 0.0298 & 0.0121 \end{pmatrix} \quad (26)$$

IV. DEPENDENCE OF EXCHANGES ON INTERACTION PARAMETERS

In this section, we give more examples of the dependence of the exchanges considered in the main text on the interaction parameters. This is done to emphasize the fact that for reasonable values of these parameters, there is a fairly large variance in the exchanges.

A. CoTiO₃

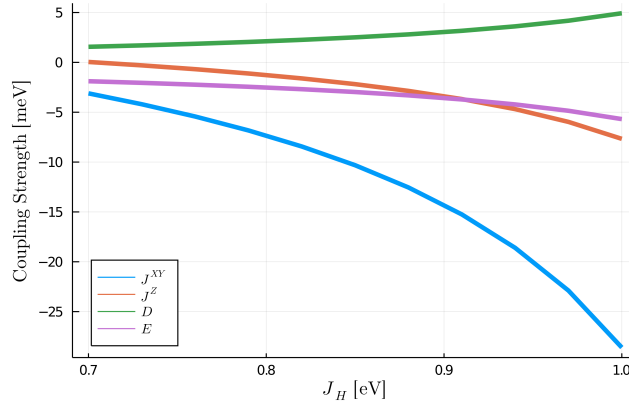


FIG. 1. Variance of 1NN Exchanges with Hund's Coupling J_H

B. $\text{BaCo}_2(\text{AsO}_4)_2$ and $\text{BaCo}_2(\text{PO}_4)_2$

The Barium compounds show similar behaviour, so the results will only be presented for $\text{BaCo}_2(\text{AsO}_4)_2$.

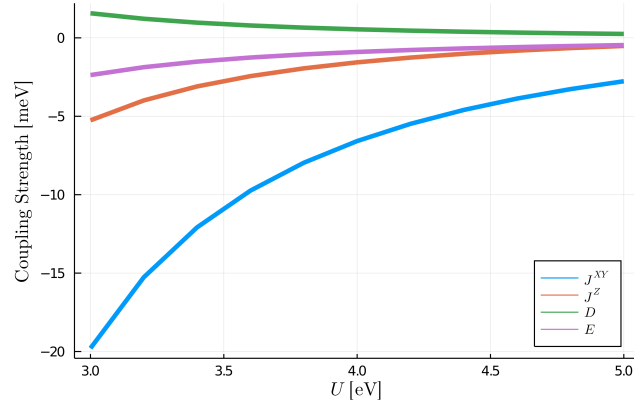


FIG. 2. Variance of 1NN Exchanges with Hubbard U

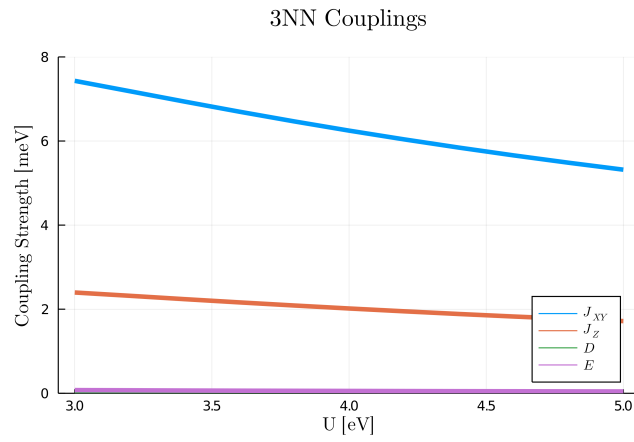


FIG. 3. Variance of 3NN Exchanges with Hubbard U

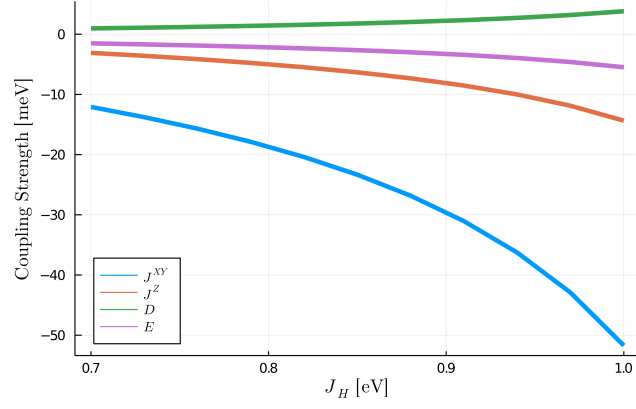


FIG. 4. Variance of 1NN Exchanges with Hund's coupling J_H

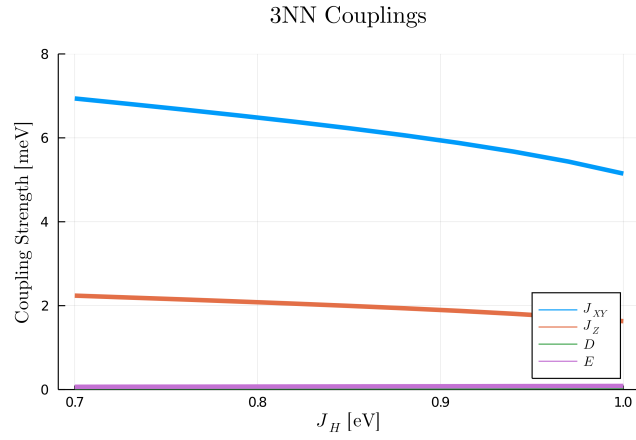


FIG. 5. Variance of 3NN Exchanges with Hund's coupling J_H

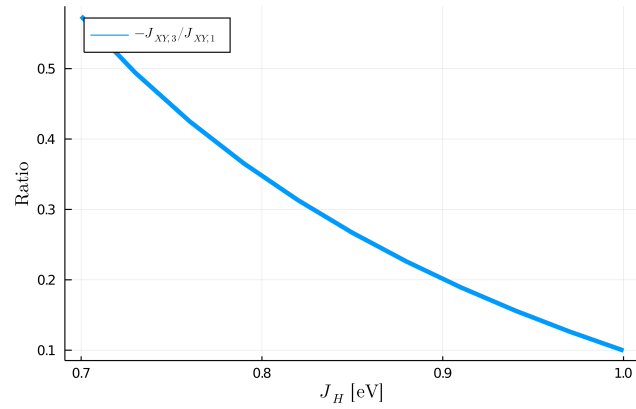


FIG. 6. Variance of the ratio $-J_3^{XY} / J_1^{XY}$ with Hund's coupling J_H

-
- [1] G. Kresse and J. Furthmüller, “Efficient iterative schemes for ab initio total-energy calculations using a plane-wave basis set,” *Phys. Rev. B* **54**, 11169–11186 (1996).
 - [2] O. K. Andersen and O. Jepsen, “Explicit, first-principles tight-binding theory,” *Phys. Rev. Lett.* **53**, 2571–2574 (1984).
 - [3] O. K. Andersen and T. Saha-Dasgupta, “Muffin-tin orbitals of arbitrary order,” *Phys. Rev. B* **62**, R16219–R16222 (2000).
 - [4] John P. Perdew, Kieron Burke, and Matthias Ernzerhof, “Generalized gradient approximation made simple,” *Phys. Rev. Lett.* **77**, 3865–3868 (1996).
 - [5] A. I. Liechtenstein, V. I. Anisimov, and J. Zaanen, “Density-functional theory and strong interactions: Orbital ordering in mott-hubbard insulators,” *Phys. Rev. B* **52**, R5467–R5470 (1995).
 - [6] Lei Wang, Thomas Maxisch, and Gerbrand Ceder, “Oxidation energies of transition metal oxides within the GGA + U framework,” *Phys. Rev. B* **73**, 195107 (2006).
 - [7] Marçal Capdevila-Cortada, Zbigniew Lodziana, and Nuria Lopez, “Performance of dft+u approaches in the study of catalytic materials,” *ACS Catalysis* **6**, 8370–8379 (2016), <https://doi.org/10.1021/acscatal.6b01907>.